Visible and Infrared Nanocrystal-based Light Modulator with CMOS Compatible Bias Operation

Huichen Zhang, Victor Guilloux, Erwan Bossavit, Ningyuan Fu, Corentin Dabard, Mariarosa Cavallo, Tung Huu Dang, Adrien Khalili, Claire Abadie, Rodolphe Alchaar, et al.

Visible and Infrared Nanocrystal-based Light Modulator with CMOS Compatible Bias Operation

Huichen Zhang[1], Victor Guilloux[1], Erwan Bossavit[1], Ningyuan Fu[2], Corentin Dabard[2], Mariarosa Cavallo[1], Tung Huu Dang[1], Adrien Khalili[1], Claire Abadie[1], Rodolphe Alchaar[1], Charlie Gréboval[1], Xiang Zhen Xu[2], James K. Utterback[1], Debora Pierucci[1], Sandrine Ithurria[2], Juan I. Climente[3], Thierry Barisien[1], Emmanuel Lhuillier[1*]

[1] Sorbonne Université, CNRS, Institut des NanoSciences de Paris, INSP, F-75005 Paris, France.
[2] Laboratoire de Physique et d'Etude des Matériaux, ESPCI-Paris, PSL Research University, Sorbonne Université Univ Paris 06, CNRS UMR 8213, 10 rue Vauquelin 75005 Paris, France.
[3] Departament de Quimica Fisica i Analitica, Universitat Jaume I, E-12080, Castello de la Plana, Spain

Abstract: Nanocrystals are now established light sources, and as synthesis and device integration have gained maturity, new functionalities can now be considered. So far, the emitted light from a nanocrystal population remains mostly driven by the structural properties (composition, size, shape) of the particle, and only limited post-synthesis tunability has been demonstrated. Here, we explore the design of light amplitude modulators using a nanocrystal-based light-emitting diode operated under reverse bias. We demonstrate strong photoluminescence modulations for devices operating in the visible and near telecom wavelengths using low bias operations (<3 V) compatible with conventional electronics. For a visible device based on 2D nanoplatelets, we demonstrate that the photoluminescence quenching is driven by the field-induced change of non-radiative decay rate and that the field is less involved than the particle charging. This work demonstrates that a simple diode stack can combine several functionalities (light emitting diode, detector, and light modulator) simply by selecting the driving bias.

Keywords: light modulator, nanocrystal, nanoplatelets, device.

*To whom correspondence should be sent: el@insp.upmc.fr

INTRODUCTION

Nanocrystals (NCs) synthesis has now gained maturity, allowing one to obtain a broad range of materials with shape control while mixing them into complex heterostructures. Thus, their integration becomes possible in a large variety of optical and optoelectronic devices, including light downconverters for display and farming,[1] single photon emission,[2,3] light emitting diodes (LED), lasers,[4] field effect transistors (FET)[5,6] solar cells[7] and cameras.[8,9]

However, among devices that remain underexplored, there is light modulator. In such devices, the input light is modulated in amplitude, phase, or frequency through an electrical knob. A common strategy to design such a light modulator relies on the Stark effect across a quantum well heterostructure. Applying an electric field across a confined heterostructure induces both a spectral redshift and a broadening of the spectrum, while the low charge displacement enables high-speed (several tens of GHz[10]) operations. In colloidal confined nanocrystals,[11] the Stark effect has also been implemented to observe potential propagation along nerves[12,13] or as a strategy to tune the spectra.[14] However, its effect in nanocrystals remains weak as the linewidth of the optical feature, which is mainly driven by inhomogeneous broadening (*i.e.,* particle size distribution), is large compared to the Stark effect-induced spectral shift.[14]

It remains that this large electric field regime of operation where the Stark effect is at play is also relevant for LEDs, since it corresponds to their high current injection regime where the efficiency droop takes place. Wood's and Bulovic's[15,16] group, at an early age of the NC-based LEDs, investigated the field-induced quenching of the luminescence as a possible mechanism to explain why NC-based LEDs were initially presenting low external quantum efficiency. In this case, the effect of the field was considered detrimental since it limited the LED performances. More recently, Xie *et al.*[17] reported the observation of strong photoluminescence (PL) quenching by a factor of 200 in a diode stack operated under reverse bias. However, the effect was only observed under a large negative bias (-20 V), which is incompatible with traditional CMOS electronics. Though certainly unoptimized, this device demonstrated that a single diode stack could provide multiple functionalities from electroluminescence (EL) under forward bias, to detector, typically around 0 V, and finally, as a light modulator under negative bias. This work further raises the question of how general this approach was and what strategies should be used to reduce the operating bias or expand the spectral wavelength of operation.

In this work, we start by investigating how a reverse bias operation of LEDs based on 2D nanoplatelets (NPLs) can be used as a light photoluminescence amplitude modulator. Among nanocrystals, 2D NPLs offer a reduced inhomogeneous broadening[18] compatible with the observation of a spectral shift induced by the Stark effect. By designing a diode stack around these NPLs, we demonstrate bias-induced PL quenching while only driving the device under 3 V. We then investigate the mechanism beyond the operation of the modulator. Using a combination of time-resolved PL, *k.p* modelling, and a model device without charge conduction, we concluded that the observed PL quenching is not driven by a Stark effect mechanism but results from the NPLs charging. In the last part of the paper, we also explore the potential of this strategy in the design of infrared modulators, and we also observe significant PL quenching (at least 80 %), while biases as low as 2 V are used to drive a LED operated near telecom wavelengths.

DISCUSSION AND RESULTS

We start by growing CdSe NPLs with a 4.5 ML thickness presenting an exciton at 510 nm. The synthesis parameters are chosen to minimize the lateral extension (around 15x15 nm^2, see **Figure 1**a) of the NPL, which presents two benefits. First, this preserves the colloidal stability of the NPL and eases the fabrication of a pinhole-free layer. Secondly, it has been observed empirically that NPLs with smaller lateral extensions have a higher photoluminescence quantum yield (PLQY)[19]. We then overcoat the NPLs with a thin ZnS shell (1 nm thick[20,21]), see the inset of **Figure 1**a. This last procedure shifts the band edge emission to around 630 nm, see **Figure 1**d.

These NPLs are then introduced into a diode stack, initially proposed for core-shell NCs[22] and later applied to NPLs.[23] In this stack, a NPL layer is sandwiched between an Ag/ZnO electron injector layer and a polyTPD/PVK/PEDOT:PSS/ITO hole injector stack, see a schematic in **Figure 1**b and energy diagram in Figure S1. Under forward bias applications, the LED displays a bright red luminescence (**Figure 1**c), with a spectrum matching the PL spectrum of the NPL,[20,24] see **Figure 1**e. This LED displays a modest electroluminescence quantum efficiency, around 2.5 % (see Figure S2), compared to state-of-the-art NPL-based LEDs.[24] However, it presents a reduced turn-on voltage (below 2 V) since this diode shows a sub-bandgap operation,[25,26] see **Figure 1**f, meaning that the bias drop is mostly occurring over the active layer (*i.e.,* ETL and HTL resistivity and thickness avoid useless bias drop).

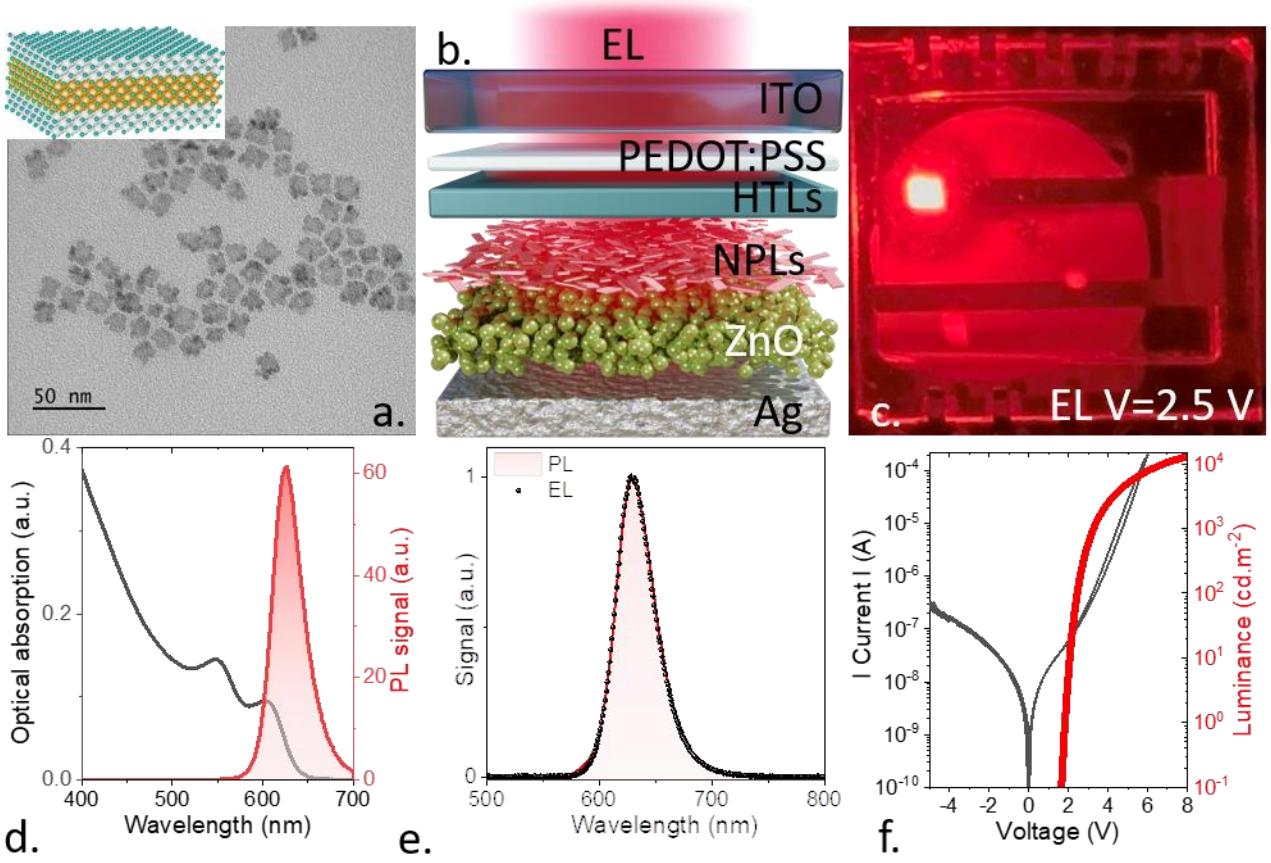

Figure 1. NPL-based LED stack. (a) Transmission electron microscopy image of CdSe/ZnS NPLs. The inset is a schematic of a single core-shell NPL. (b) Schematic of the NPL-based LED stack. (c) Image of the LED stack under forward bias highlighting the emission of the red electroluminescence signal. (d) Absorption and photoluminescence spectra of the CdSe/ZnS NPL. (e) Photoluminescence spectrum of the CdSe/ZnS NPL and electroluminescence spectrum from the NPL-based LED stack. (f) Current and luminance from NPL-based LED stack as a function of the applied bias.

We have also checked that under 0 V operation, the diode stack can be used as a photovoltaic light detector, see Figure S3, even though the performances are sub-optimal due to the low absorption of the structure.

More interestingly, we tested the potential of this LED stack as a PL modulator. To do so, a blue (405 nm) laser is shone on the LED, and reverse bias is applied on the pixel, see **Figure 2**a-b and video S1. We observe a strong PL quenching on the corresponding pixel, see **Figure 2**b-c. Under -3 V, the PL drop can reach a factor 30 (**Figure 2**d).

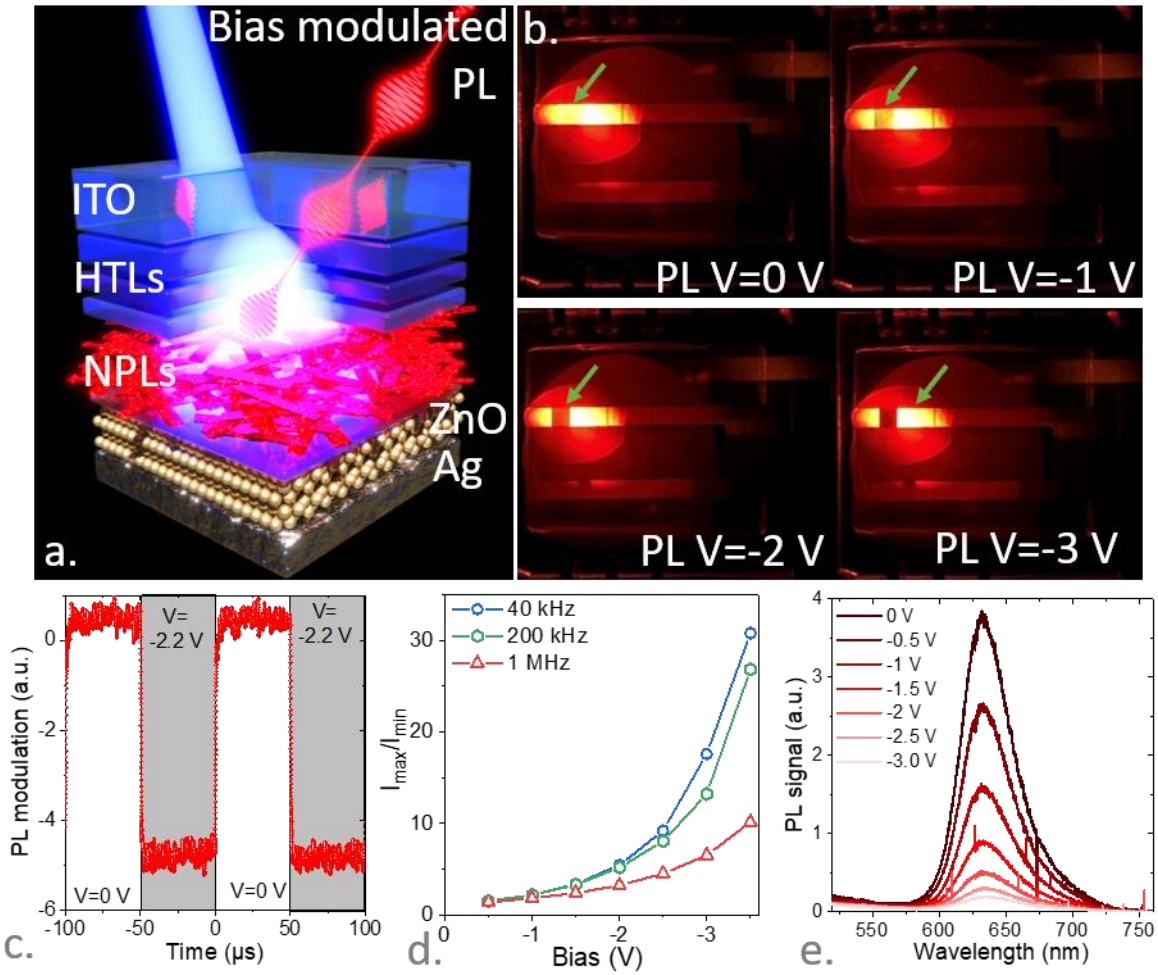

Figure 2. LED stack used as a light modulator. (a) schematic of the LED stack used to modulate the PL magnitude. (b) Images of the NPL-based LED stack under illumination by a blue laser, while various reverse bias voltages are applied on the pixel highlighted by an arrow. The larger the applied reverse bias, the weaker the PL signal from this area. (c) Change in the PL signal resulting from the application of a negative bias pulse as a function of time. (d) Modulation of the PL amplitude (ratio of the signal with and without bias) as a function of the applied reverse bias for various frequency modulations. (e) PL spectra, coming from the pixel area, under various applied reverse biases. Also see Figure S4 for normalized spectra.

Beyond the obvious drop of the magnitude (**Figure 2**d), the PL spectrum appears to be marginally affected. The normalized spectra (Figure S4a-b), in particular, do not display a significant redshift, as would have been anticipated if the Stark effect was at play. Under reverse bias application, the PL decay becomes faster, see **Figure 3**a-b and S5. However, the decay time is only 4 times faster under -3 V, whereas the PL magnitude drops by a factor of 30. The PL efficiency, being related to the ratio of radiative and non-radiative lifetimes, may directly be affected by a field-induced change of the wave function overlap. Using *k.p* simulations[27] (see supporting information section 6), we

have determined the excitonic wave function (**Figure 3**c-d and S9) in these core-shell NPLs under zero field and a large field F=2 MV.cm^{-1}, a value 10 times larger than the average electric field to account for possible field inhomogeneity. Under an electric field application, both electron and hole wave functions tend to localize in the triangular parts of their respective wells, reducing their overlap. Since the radiative decay rate scales with this overlap, we expect the radiative lifetime to increase with the field application, see **Figure 3**e. However, this lifetime increase is weak in practice: around 1 % at 200 kV.cm^{-1} (average field assuming 3 V is applied) and around 15 % at 2000 kV.cm^{-1} (a value 10 times larger than the average field to consider an inhomogeneous energy drop in the structure). Firstly, the experimental shortening of the PL decay time is contradictory with a Stark effect-mediated increase of the radiative lifetime. Meanwhile, the weak shift for the exciton energy resulting from the simulation, as shown, see **Figure 3**e, is consistent with the lack of experimental shift, as observed in **Figure 2**e and S4b.

Secondly, the lengthening of the radiative lifetime (less than 15 %) is too small to account for the significant drop in the PL quantum yield. Together, these points suggest that the decrease in PL quantum yield is primarily the result of the shortening of the non-radiative lifetime. Third, though the effect is too small to explain the PL quenching under reverse bias, the longer radiative recombination time is definitely a mechanism at play also under forward bias and involved in the LED external quantum efficiency (EQE) droop observed under large current injection.

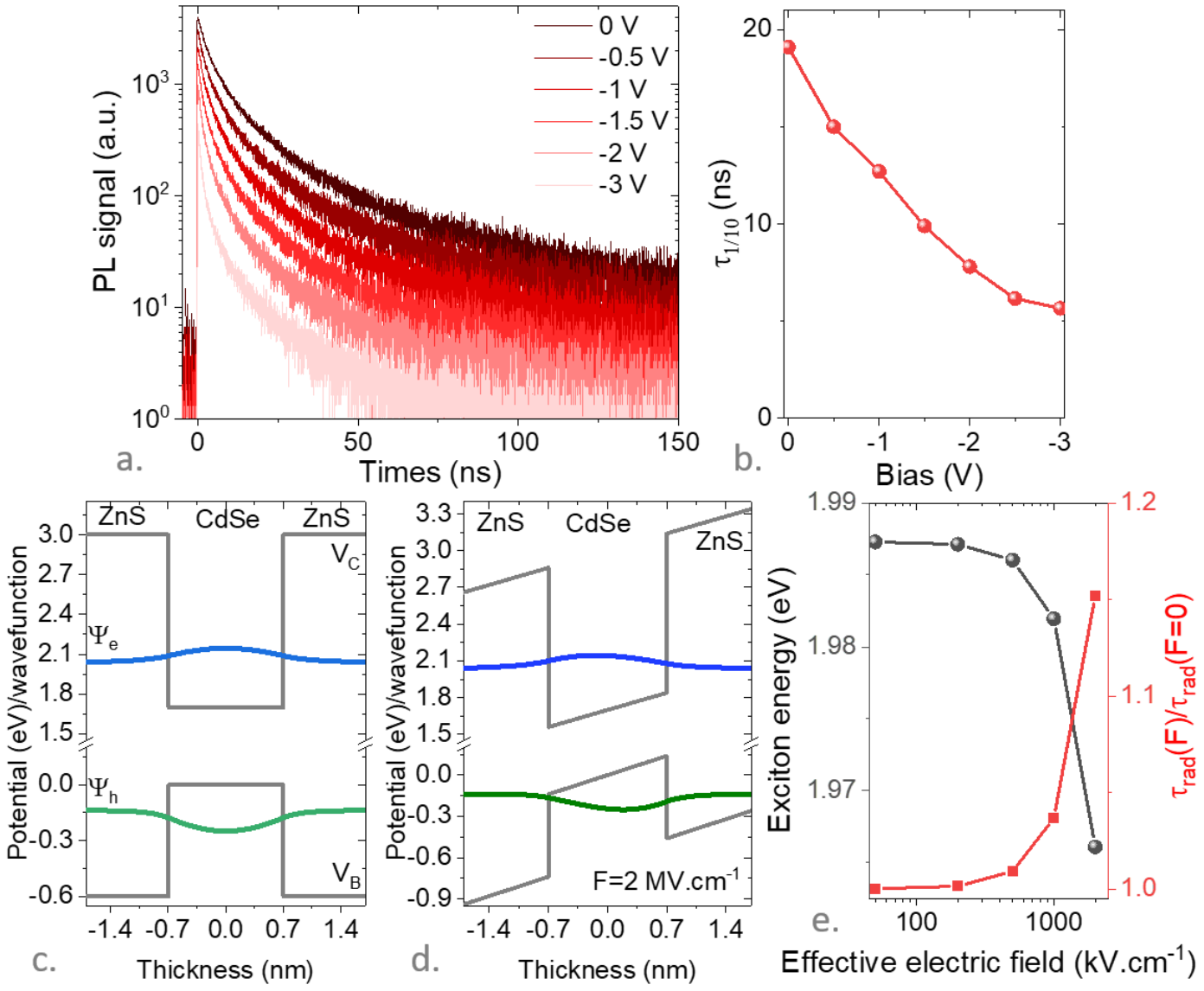

Figure 3. Impact of the electric field on the carrier dynamics. (a). PL signal as a function of time for various applied reverse biases. (b). Time for the PL magnitude to drop by one order of magnitude as a function of time for various applied reverse biases. (c) (resp (d)) Conduction and valence band energy profiles (in grey), as well as the electron (blue) and hole (green) wavefunctions for the CdSe/ZnS NPL under null (resp 2 $MV.cm^{-1}$) electric field perpendicular to the NPL plane. For the sake of clarity, the wavefunctions have been shifted to their eigenenergy. (e) Simulated exciton energy and ratio of the radiative lifetime (see discussion in SI) under a given electric field over the radiative lifetime under zero field as a function of the effective electric field along the NPL thickness.

The bias-induced modulation of the PL magnitude appears to be driven by the change in the non-radiative decay process. Concomitant with the change of the wavefunction overlap, the field pushes the wave functions toward the surface of the nanocrystals, making them experience surface traps. Though this contribution may be drastically reduced in a core-shell structure, such an effect will also compete with particle charging. To disentangle the effect of pure electric field from particle charging resulting from a current injection, we compare the effect of bias application in the LED stack and in a model system, where the same electrodes are used but where the diode stack is replaced by a blend of NPL in a transparent dielectric medium (here PMMA). The field can be applied in the latter structure, but the current passing through the structure decreases below the setup resolution, as shown by the IV curves of the two devices, see **Figure 4**a. In the previous diode stack, apparent PL modulation is observed under a moderate electric field, while in the case of the NPL embedded in the dielectric, no PL modulation is observed even under large field. We can thus conclude that, in this structure, PL quenching is connected to charge injection, which contrasts with the result by Xie *et al.*, for which the higher driving voltage enables a more effective Stark effect[17]. Charging may also induce fast Auger recombination (100 ps in CdS NPL), that can be faster than our dynamics setup resolution, which may explain why the drop in dynamics appears smaller than the one of the PL efficiency.

The involvement of charging is further reinforced by the moderate speed of the PL switch, see **Figure *2***d, which presents a cut-off frequency between 100 kHz and 1 MHz. This cut-off frequency seems incompatible with the expected fast operation of a Stark in which there is no charge injection. From previous study, based on X ray photoemission, the NPL made of CdSe/ZnS structure have been shown to present a *n*-type character,[28] with a Fermi level in the upper part of the band gap. Thus, the formed charged species are likely negative trions and higher order multi exciton.

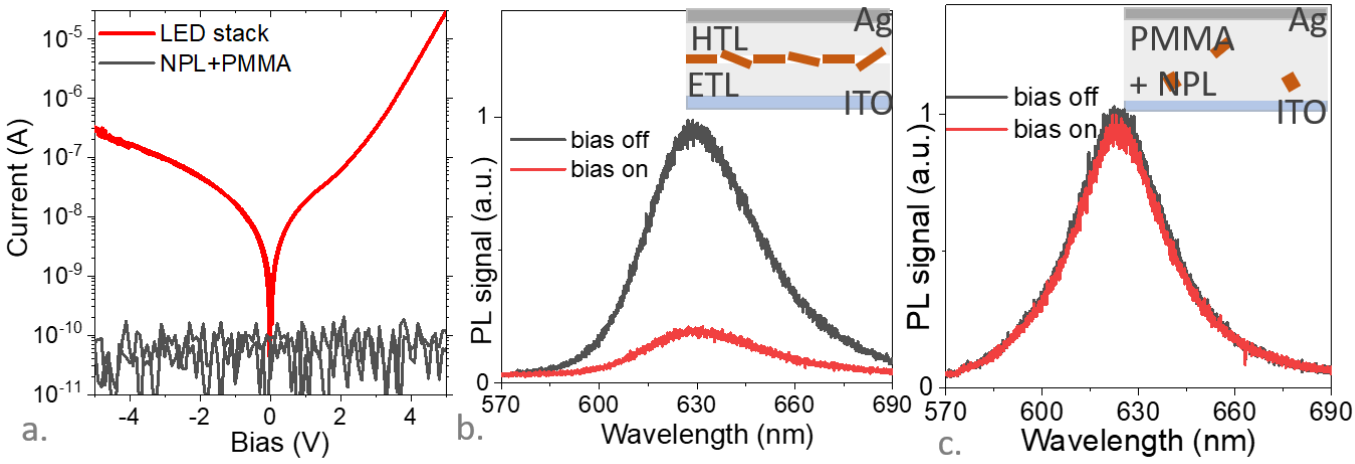

Figure 4. Pure effect of the electric field. (a) IV curves for the NPL-based LED stack and for a device made of the same contacts but in which the inner layer is made of a NPL/PMMA mixture. (b) PL spectra when the negative bias is turned on and off for the NPL-based LED stack. (c) PL spectra when the negative bias is turned on and off for the device made of the same contacts but in which the inner layer is made of a NPL/PMMA mixture.

In the last part of the paper, we have explored if this concept of LED stack operated under reverse bias as a light modulator can be extended to the infrared. In this case, we use the diode stack proposed by Qu *et al.*[29], in which the active medium is made of HgTe NCs presenting emission at around 1.3 µm. The aforementioned stack is inspired from previous work by Pradhan *et al*.[30] The *n*- and *p*-sides of the junction rely respectively on well-established layers of ZnO and EDT-capped PbS NCs, which are commonly used for solar cells.[31,32] The active layer is made of a blend of HgTe (see Figure S6) and ZnO NCs. This blend forms a bulk heterojunction in which the ZnO carries electron and HgTe the holes. The ratio of the two materials is used to adjust the charge balance.[29] A scheme of the structure is proposed in **Figure 5**a.

The diode shows EL signal under forward operation as shown by an infrared image of the diode under positive bias application, see top left image of **Figure 5**c and S7 for additional characterization of the infrared LED. Under illumination, we also observe a PL signal modulation as reverse bias is applied, see movie S2. The latter already reaches 80 % under -2V, see **Figure 5**b-c and S8. This last result further confirms that light modulators can be obtained from most diode stacks operated under reverse bias.

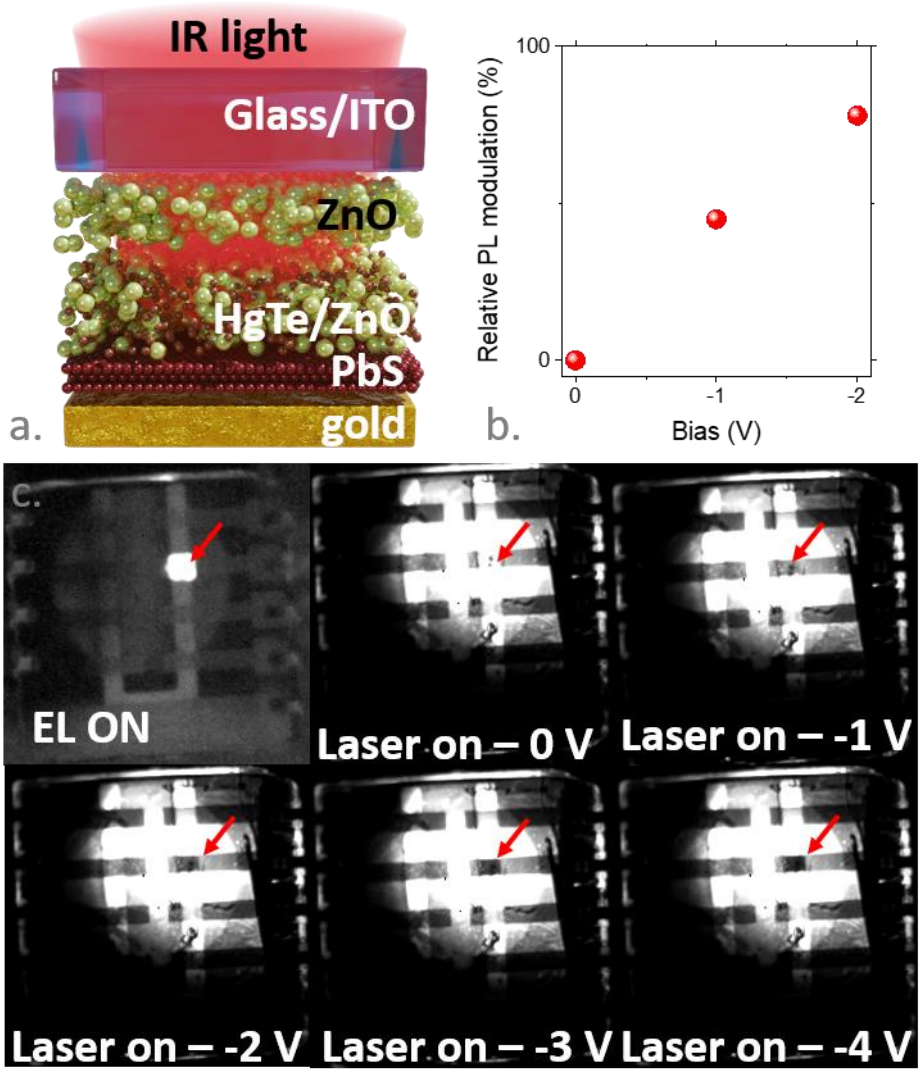

Figure 5. Infrared light modulation in a narrow band gap LED stack. (a) Schematic of the LED stack in which the emitting medium is made of HgTe NCs. (b) Relative modulation of the PL signal as a function of the applied reverse bias. (c) Images of the HgTe NC-based LED stack, obtained from an InGaAs camera (NIT 1601), under illumination by a 405 nm laser, while various reverse biases are applied on the pixel highlighted by an arrow.

CONCLUSION

We demonstrate light modulators presenting strong light modulation (a factor of 30 in the visible and 80 % in the IR) under low bias operation (3 V and below) from a conventional LED stack. In the case of a NPL-based LED, we demonstrate that the PL quenching is mainly driven by the change of the non-radiative decay dynamics. Moreover, we show that the PL quenching is less dictated by the electric field magnitude than by the current passing in the structure. This clearly suggests that the additional non-radiative decay pathway at play under reverse bias operation is connected to the formation of charged species. This mechanism enables large current modulation under low field operation but comes at the price of a slower dynamics compared to more conventional Stark modulators.

ASSOCIATED CONTENT

Supporting Information

The Supporting Information is available free of charge at

Supporting information include nanocrystal synthesis and LED fabrication procedure, visible and infrared device characterization and *k.p* modelling for the NPL heterostructure.

SI also include video of the visible (video S1: LED visible file) and infrared (video S2: LED IR file) modulator under operation.

COMPETING INTEREST

The authors declare no competing financial interest.

FUNDING SOURCES

The project is supported by ERC starting grant blackQD (grant n° 756225) and Ne2Dem (grant n° 853049). We acknowledge the use of clean-room facilities from the “Centrale de Proximité Paris-Centre”. This work has been supported by the Region Ile-de-France in the framework of DIM Nano-K (grant dopQD). This work is supported by French state funds managed by the ANR within the Investissements d'Avenir programme under reference ANR-11-IDEX-0004-02, and more specifically within the framework of the Cluster of Excellence MATISSE and also by the grant IPER-Nano2 (ANR-18CE30-0023-01), Copin (ANR-19-CE24-0022), Frontal (ANR-19-CE09-0017), Graskop (ANR-19-CE09-0026) and NITQuantum (ANR-20-ASTR-0008-01), Bright (ANR-21-CE24-0012-02), MixDferro (ANR-21-CE09-0029) and QuickTera (ANR-22-CE09-0018). JIC acknowledge support from UJI-B2021-06 and MICINN PID2021-128659NB-I00. H.Z. thanks China Scholarship Council for Ph.D. funding.

REFERENCES

(1) Erdem, T.; Demir, H. V. Colloidal Nanocrystals for Quality Lighting and Displays: Milestones and Recent Developments. *Nanophotonics* **2016**, *5*, 74–95.

(2) Correa, R. E.; Dauler, E. A.; Nair, G.; Pan, S. H.; Rosenberg, D.; Kerman, A. J.; Molnar, R. J.; Hu, X.; Marsili, F.; Anant, V.; Berggren, K. K.; Bawendi, M. G. Single Photon Counting from Individual Nanocrystals in the Infrared. *Nano Lett.* **2012**, *12*, 2953–2958.

(3) Brokmann, X.; Giacobino, E.; Dahan, M.; Hermier, J. P. Highly Efficient Triggered Emission of Single Photons by Colloidal CdSe⁄ZnS Nanocrystals. *Appl. Phys. Lett.* **2004**, *85*, 712–714.

(4) Park, Y.-S.; Roh, J.; Diroll, B. T.; Schaller, R. D.; Klimov, V. I. Colloidal Quantum Dot Lasers. *Nat. Rev. Mater.* **2021**, *6*, 382–401.

(5) Talapin, D. V.; Murray, C. B. PbSe Nanocrystal Solids for n- and p-Channel Thin Film Field-Effect Transistors. *Science* **2005**, *310*, 86–89.

(6) Hetsch, F.; Zhao, N.; Kershaw, S. V.; Rogach, A. L. Quantum Dot Field Effect Transistors. *Mater. Today* **2013**, *16*, 312–325.
(7) Carey, G. H.; Abdelhady, A. L.; Ning, Z.; Thon, S. M.; Bakr, O. M.; Sargent, E. H. Colloidal Quantum Dot Solar Cells. *Chem. Rev.* **2015**, *115*, 12732–12763.
(8) Gréboval, C.; Darson, D.; Parahyba, V.; Alchaar, R.; Abadie, C.; Noguier, V.; Ferré, S.; Izquierdo, E.; Khalili, A.; Prado, Y.; Potet, P.; Lhuillier, E. Photoconductive Focal Plane Array Based on HgTe Quantum Dots for Fast and Cost-Effective Short-Wave Infrared Imaging. *Nanoscale* **2022**, *14*, 9359–9368.
(9) Rauch, T.; Böberl, M.; Tedde, S. F.; Fürst, J.; Kovalenko, M. V.; Hesser, G.; Lemmer, U.; Heiss, W.; Hayden, O. Near-Infrared Imaging with Quantum-Dot-Sensitized Organic Photodiodes. *Nat. Photonics* **2009**, *3*, 332–336.
(10) Dely, H.; Bonazzi, T.; Spitz, O.; Rodriguez, E.; Gacemi, D.; Todorov, Y.; Pantzas, K.; Beaudoin, G.; Sagnes, I.; Li, L.; Davies, A. G.; Linfield, E. H.; Grillot, F.; Vasanelli, A.; Sirtori, C. 10 Gbit s $^{-1}$ Free Space Data Transmission at 9 µm Wavelength With Unipolar Quantum Optoelectronics. *Laser Photonics Rev.* **2022**, *16*, 2100414.
(11) Rowland, C. E.; Currie, M.; Susumu, K.; Oh, E.; Kushto, G.; Efros, A. L.; Huston, A. H.; Delehanty, J. B. Effects of Shell Thickness on the Electric Field Dependence of Exciton Recombination in CdSe/CdS Core/Shell Quantum Dots. *Opt. Mater. Express* **2017**, *7*, 1871.
(12) Efros, A. L.; Delehanty, J. B.; Huston, A. L.; Medintz, I. L.; Barbic, M.; Harris, T. D. Evaluating the Potential of Using Quantum Dots for Monitoring Electrical Signals in Neurons. *Nat. Nanotechnol.* **2018**, *13*, 278–288.
(13) Rowland, C. E.; Susumu, K.; Stewart, M. H.; Oh, E.; Mäkinen, A. J.; O'Shaughnessy, T. J.; Kushto, G.; Wolak, M. A.; Erickson, J. S.; L. Efros, A.; Huston, A. L.; Delehanty, J. B. Electric Field Modulation of Semiconductor Quantum Dot Photoluminescence: Insights Into the Design of Robust Voltage-Sensitive Cellular Imaging Probes. *Nano Lett.* **2015**, *15*, 6848–6854.
(14) Scott, R.; Achtstein, A. W.; Prudnikau, A. V.; Antanovich, A.; Siebbeles, L. D. A.; Artemyev, M.; Woggon, U. Time-Resolved Stark Spectroscopy in CdSe Nanoplatelets: Exciton Binding Energy, Polarizability, and Field-Dependent Radiative Rates. *Nano Lett.* **2016**, *16*, 6576–6583.
(15) Bozyigit, D.; Wood, V.; Shirasaki, Y.; Bulovic, V. Study of Field Driven Electroluminescence in Colloidal Quantum Dot Solids. *J. Appl. Phys.* **2012**, *111*, 113701.
(16) Bozyigit, D.; Yarema, O.; Wood, V. Origins of Low Quantum Efficiencies in Quantum Dot LEDs. *Adv. Funct. Mater.* **2013**, *23*, 3024–3029.
(17) Xie, S.; Zhu, H.; Li, M.; Bulović, V. Voltage-Controlled Reversible Modulation of Colloidal Quantum Dot Thin Film Photoluminescence. *Appl. Phys. Lett.* **2022**, *120*, 211104.
(18) Tessier, M. D.; Javaux, C.; Maksimovic, I.; Loriette, V.; Dubertret, B. Spectroscopy of Single CdSe Nanoplatelets. *ACS Nano* **2012**, *6*, 6751–6758.
(19) Di Giacomo, A.; Rodà, C.; Khan, A. H.; Moreels, I. Colloidal Synthesis of Laterally Confined Blue-Emitting 3.5 Monolayer CdSe Nanoplatelets. *Chem. Mater.* **2020**, *32*, 9260–9267.
(20) Kelestemur, Y.; Shynkarenko, Y.; Anni, M.; Yakunin, S.; De Giorgi, M. L.; Kovalenko, M. V. Colloidal CdSe Quantum Wells with Graded Shell Composition for Low-Threshold Amplified Spontaneous Emission and Highly Efficient Electroluminescence. *ACS Nano* **2019**, *13*, 13899–13909.
(21) Heuclin, H.; Nadal, B.; Grazon, C.; Mahler, B.; Lhuillier, E. Core-Shell Nanoplatelets Film and Display Device Using the Same. WO 2016156266 A1, October 6, 2016.
(22) Dai, X.; Zhang, Z.; Jin, Y.; Niu, Y.; Cao, H.; Liang, X.; Chen, L.; Wang, J.; Peng, X. Solution-Processed, High-Performance Light-Emitting Diodes Based on Quantum Dots. *Nature* **2014**, *515*, 96–99.
(23) Qu, J.; Rastogi, P.; Gréboval, C.; Livache, C.; Dufour, M.; Chu, A.; Chee, S.-S.; Ramade, J.; Xu, X. Z.; Ithurria, S.; Lhuillier, E. Nanoplatelet-Based Light-Emitting Diode and Its Use in All-Nanocrystal LiFi-like Communication. *ACS Appl. Mater. Interfaces* **2020**, *12*, 22058–22065.
(24) Liu, B.; Altintas, Y.; Wang, L.; Shendre, S.; Sharma, M.; Sun, H.; Mutlugun, E.; Demir, H. V. Record High External Quantum Efficiency of 19.2% Achieved in Light-Emitting Diodes of Colloidal Quantum Wells Enabled by Hot-Injection Shell Growth. *Adv. Mater.* **2020**, *32*, 1905824.

(25) Pradhan, S.; Dalmases, M.; Konstantatos, G. Origin of the Below-Bandgap Turn-On Voltage in Light-Emitting Diodes and the High V_{OC} in Solar Cells Comprising Colloidal Quantum Dots with an Engineered Density of States. *J. Phys. Chem. Lett.* **2019**, *10*, 3029–3034.
(26) Luo, H.; Zhang, W.; Li, M.; Yang, Y.; Guo, M.; Tsang, S.-W.; Chen, S. Origin of Subthreshold Turn-On in Quantum-Dot Light-Emitting Diodes. *ACS Nano* **2019**, *13*, 8229–8236.
(27) Rajadell, F.; Climente, J. I.; Planelles, J. Excitons in Core-Only, Core-Shell and Core-Crown CdSe Nanoplatelets: Interplay between in-Plane Electron-Hole Correlation, Spatial Confinement, and Dielectric Confinement. *Phys. Rev. B* **2017**, *96*, 035307.
(28) Cruguel, H.; Livache, C.; Martinez, B.; Pedetti, S.; Pierucci, D.; Izquierdo, E.; Dufour, M.; Ithurria, S.; Aubin, H.; Ouerghi, A.; Lacaze, E.; Silly, M. G.; Dubertret, B.; Lhuillier, E. Electronic Structure of CdSe-ZnS 2D Nanoplatelets. *Appl. Phys. Lett.* **2017**, *110*, 152103.
(29) Qu, J.; Rastogi, P.; Gréboval, C.; Lagarde, D.; Chu, A.; Dabard, C.; Khalili, A.; Cruguel, H.; Robert, C.; Xu, X. Z.; Ithurria, S.; Silly, M. G.; Ferré, S.; Marie, X.; Lhuillier, E. Electroluminescence from HgTe Nanocrystals and Its Use for Active Imaging. *Nano Lett.* **2020**, *20*, 6185–6190.
(30) Pradhan, S.; Di Stasio, F.; Bi, Y.; Gupta, S.; Christodoulou, S.; Stavrinadis, A.; Konstantatos, G. High-Efficiency Colloidal Quantum Dot Infrared Light-Emitting Diodes via Engineering at the Supra-Nanocrystalline Level. *Nat. Nanotechnol.* **2019**, *14*, 72–79.
(31) Chuang, C.-H. M.; Brown, P. R.; Bulović, V.; Bawendi, M. G. Improved Performance and Stability in Quantum Dot Solar Cells through Band Alignment Engineering. *Nat Mater* **2014**, *13*, 796–801.
(32) Lu, K.; Wang, Y.; Liu, Z.; Han, L.; Shi, G.; Fang, H.; Chen, J.; Ye, X.; Chen, S.; Yang, F.; Shulga, A. G.; Wu, T.; Gu, M.; Zhou, S.; Fan, J.; Loi, M. A.; Ma, W. High-Efficiency PbS Quantum-Dot Solar Cells with Greatly Simplified Fabrication Processing via “Solvent-Curing.” *Adv. Mater.* **2018**, *30*, 1707572.

TOC graphic

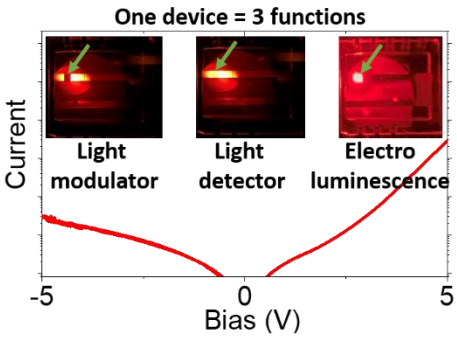
One device = 3 functions
Light modulator
Light detector
Electro luminescence
Current
-5
0
5
Bias (V)